Dig Dis Sci (2014) 59:1169–1179
DOI 10.1007/s10620-014-3168-5

ORIGINAL ARTICLE

NOD-*scidIl2rg*^{tm1Wjl} and NOD-*Rag1*^{null}*Il2rg*^{tm1Wjl}: A Model for Stromal Cell–Tumor Cell Interaction for Human Colon Cancer

Justin Maykel · Jian Hua Liu · Hanchen Li · Leonard D. Shultz · Dale L. Greiner · JeanMarie Houghton

Received: 9 September 2013 / Accepted: 15 April 2014 / Published online: 6 May 2014

Abstract
Background/Aims Stromal cells and the extracellular environment are vital to human tumors, influencing growth and response to therapy. Human tumor cell lines lack stroma and transplantation into immunodeficient mice does not allow meaningful analyses of the effects of stroma on tumor cell growth. Studies of xenografts of primary human tumor fragments in nude mice and in early *scid* mouse models were constrained by poor tumor growth accompanied by host-versus-graft reactivity, dramatically altering tumor architecture and tumor microenvironment. In contrast, severely immunodeficient NOD-*scid* and NOD-*Rag1*^{null} strains carrying the *IL2rg*^{null} mutation (NSG and NRG) support the growth of many types of human primary tumors.

Methods/Results We compared the take rate, growth and architectural preservation of 10 clinically distinct primary human colon cancers in NOD-*scid*, NOD-*Rag1*^{null}, NSG and NRG mice and determined the contribution of mouse and human cells to the stroma during tumor proliferation and expansion in secondary hosts and tumor response to treatment with 5-fluorouracil (5-FU). NSG and NRG mice more readily support growth of human primary colon tumor fragments than do NOD-*scid*, NOD-*Rag1*^{null} mice and maintain tumor architectural integrity in the primary recipient and through subsequent transplant generations. The human colon tumors were responsive to treatment with 5-FU. Human stromal cells in the primary graft were replaced by mouse-derived fibroblasts in a dynamic process during subsequent passages.
Conclusion Human colon cancer xenografts propagated in NSG and NRG mice maintain structural fidelity while replacing human stromal cells with murine stromal cells.

Keywords NSG · NRG · Immunodeficient mouse models · Human colon cancer · Tumor stroma

J. Maykel
Division of Colorectal Surgery, Department of Surgery, UMass Memorial Health Care System, Worcester, MA, USA

J. H. Liu · H. Li · J. Houghton (✉)
Division of Gastroenterology, Department of Medicine, LRB Second Floor-209, University of Massachusetts Medical School, 364 Plantation Street, Worcester, MA 01635, USA
e-mail: jeanmarie.houghton@umassmed.edu

L. D. Shultz
The Jackson Laboratory, 600 Main Street, Bar Harbor, ME, USA

D. L. Greiner
Program in Molecular Medicine, Diabetes Center of Excellence, University of Massachusetts Medical School, Worcester, MA, USA

J. Houghton
Department of Cancer Biology, University of Massachusetts Medical School, Worcester, MA, USA

Introduction

Immunodeficient mouse models that are able to engraft human tumor specimens are crucial for studying the complex interaction between cancer cells, stroma and the human immune system in vivo. Hypoxia [1], stromal cells themselves [2] and elaborated factors from the activated stroma [3, 4] are central players in the initiation and progression of epithelial cancers [5]. The tumor stroma coordinates and orchestrates many of the invasive and metastatic properties of cancer [6–8], making stroma a promising target for therapeutic interventions. A significant

roadblock to understanding the tumor–stromal interaction in human colon cancer has been the lack of a human tumor model that can be manipulated and stringently interrogated in vivo. Growth of human tissue, especially human tumors, in mouse models has been problematic for many reasons. Commonly used immunodeficient mice include those carrying the severe combined immunodeficiency (*Prkdc*^{scid}, abbreviated as *scid*) mutation as well as mice deficient in the recombination activating genes 1 or 2 (*Rag1*^{null} or *Rag2*^{null}). These immunodeficient mouse models have moderate natural killer (NK) cell activity and other innate immune function that impede primary human tumor engraftment. Perhaps as important as the low level of engraftment of the tumors is destruction of tumor architecture, loss of stromal integrity and rejection of tumors that showed initial engraftment. These models are used with some success for analyzing the growth of distinct subsets of purified cancer cells [9–11], but are less reliable when used for intact tumor fragments. Mouse host innate immune cells infiltrate into tumors, distorting the architecture, destroying cells and altering the local tumor environment dramatically. The growth rate and architectural characteristics of tumors from a single sample often differ unpredictably and dramatically within a single cohort of mice, thus hampering reproducibility of study findings [12–15]. Because of these limitations, there has been keen interest in identifying alternate mouse models for growing and analyzing primary human tumor tissue. The NOD-*scid Il2rg*^{tm1Wjl} (NSG) mouse strain has recently been identified as an ideal model for growth of primary human tumor samples [16–18].

This model allows tumor cell proliferation and maintains tumor-associated immune cells and stroma during primary tumor growth [19]. The NSG and the NOD-*Rag1*^{null}*Il2rg*^{tm1Wjl} (NRG) mouse strains lack a functional IL2 receptor common chain gene (*IL2rg*), which is required for ligand binding and high-affinity signaling through the IL2, IL4, IL7, IL9, IL15 and IL21 receptors. Therefore, NSG and NRG mice exhibit severe impairment in both innate and adaptive immunity, the combined immunologic hurdles to xenogeneic tumor cell propagation in immunodeficient mouse models. The *scid*, *Rag1*^{null} *and Rag2*^{null} mutations prevent the genetic recombination required for functional B- and T-cell receptors, resulting in similar immune defects. However, the *scid* mutation is broadly expressed and significantly impacts DNA repair in all tissues, while *Rag1*^{null} *and Rag2*^{null} mice exhibit defects restricted to recombination within T- and B-cell receptors. Because of these differences, NSG mice show increased sensitivity to radiation and potentially drug-induced DNA damage, while the NRG mice are relatively resistant. While the NSG model has been used for the study of primary human lung tumors [19] melanomas [20], ovarian [21] as well as a number of human leukemias [22, 23], there are few published reports on propagation of GI tract tumors with no data on fidelity of architecture in propagated tumors or formal interrogation of the cytokine/stromal compartment over time.

In this study, we describe the growth of primary human colon cancer fragments in the NSG and NRG models and show that tumors grow readily, reliably and maintain architectural integrity through subsequent passages. These tumors can be serially passaged up to at least five generations without loss of tumor structure. There is little if any necrosis and virtually no host inflammatory cell infiltrate noted at baseline, and the tumors are susceptible to chemotherapeutic agents used clinically for colon cancer, further supporting the notion that this is a clinically relevant model of human colon cancer. A striking feature of tumor grown in these mice is that the human stroma becomes entirely replaced by mouse-derived cells by the third transplant tumor generation.

Materials and Methods

Tumor Specimens

After all clinically needed samples were obtained, and surgical margins evaluated, the excess tumor was released to the tumor bank at the University of Massachusetts Medical School under an IRB approved protocol. Discarded colon cancer tumor specimens were obtained from the UMass Tumor bank within 1 h of surgical resection, placed in sterile PBS and transported on ice to the animal facility.

Mice

NOD.CB17-*Prkdc*^{scid}/Sz (NOD-*scid*), NOD.CB17-*Prkdc*^{scid} *Il2rg*^{tm1Wj1}/Sz (NSG), NOD.Cg-*Rag1*^{tm1Mom}/*Sz* (NOD-*Rag1*^{null}) and NOD.Cg-*Rag1*^{tm1Mom} *IL2rg*^{tm1Wjl}/Sz (NRG) mice were generated at The Jackson Laboratory. NSG mice expressing green fluorescent protein (GFP) driven by the chicken beta actin promoter (NOD.CB17-*Prkdc*^{scid} *IL2rg*^{tm1Wj1} Tg(CAG-EGFP)1Osb/Sz (abbreviated as NSG-GFP mice) were generated by crossing NSG mice with NOD.CB17-*Prkdc*^{scid} Tg(CAG-EGFP)1Osb mice followed by backcrossing the CAG-EGFP transgene onto the NSG strain. All mice were housed in a specific pathogen-free facility in microisolator cages with free access to autoclaved food and acidified water supplemented with sulfamethoxazole–trimethoprim (SMZ–TMP). All studies were approved by the Institutional Animal Care and Use Committees of the University of Massachusetts Medical School (IACUC) and at The Jackson Laboratory.

Using sterile technique, primary tumor specimens were minced and 1 mm × 1 mm tumor fragments implanted in the subrenal capsule of anesthetized NSG or NOD-*scid* mice, or subcutaneously (SC) in the right flank of anesthetized NOD-*scid*, NOD-*Rag1*^{null}, NSG, NRG or NSG-GFP mice using an 18-gauge trocar. Mice were maintained on TMP-SMZ, and tumors were allowed to grow to 0.5–1 cm in size in the largest dimension. Tumors were harvested at 2–4 weeks. A portion of each tumor was sequentially passaged into second through fifth generation mice and processed for analysis in similar fashion.

Evaluation of Tumors

At necropsy organs were visually inspected for evidence of metastasis. Primary tumors and a portion of surrounding tissue were harvested and processed for frozen sections or were formalin fixed and paraffin embedded, and 5-μm sections were prepared for standard histology and immunohistochemistry (IHC). Antibodies directed against; human vimentin (Abcam, Cambridge MA, human-specific recognition without mouse cross-reactivity), human CD45 (Abcam, Cambridge MA, human-specific recognition without mouse cross-reactivity), green fluorescence protein (GFP, Invitrogen, Grand Island, NY.), proliferating cell nuclear antigen (PCNA, Epitomics, Burlingame, CA; reacts with both human and mouse proteins) and vascular endothelial growth factor (VEGF, Abcam, Cambridge MA, reacts with both human and mouse proteins) were used according to standard protocol and detected using pre-adsorbed, biotin conjugated secondary antibody. GFP expression was also evaluated by direct fluorescence microscopy on DAPI/anti-fade prepared frozen sections.

Tolerance of Mice to 5-FU

Non-tumor-bearing NOD-*scid*, NOD-*Rag1*^{null}, NSG or NRG mice were treated daily with ip injections of 5-fluorouracil (5-FU) (5 mg/kg) for 14 days [24–27]. Mice were weighed before administration of 5-FU and daily during treatment. On day 0, 7 and 15, complete blood counts were performed. On day 15, mice were euthanized by CO_2 asphyxiation and complete necropsies were performed. Liver, small bowel and colon were fixed in 10 % formalin, processed, paraffin embedded, sectioned 5 μm and evaluated following H&E staining and IHC for PCNA to quantitate chemotherapy-induced damage and subsequent repair ($n = 6$ per group).

Response of Human Tumors to 5-FU Chemotherapy

NSG or NRG mice implanted with colon tumors were treated with 5-FU ip for 14 days at a dose of 5 mg/kg initiated once tumors were at least 0.25 × 0.25 cm in size. On days 0, 7 and 15, complete blood counts were taken and on days 7 and 15, and tumors were measured by caliper. On day 15, mice were euthanized and complete necropsies were performed. Tumors were collected, weighed and processed for histology and IHC ($n = 6$ per group).

Results

NSG and NRG Mice Support Robust Growth of Human Colon Tumors

Both NSG and NRG mice supported robust growth of human colon cancer tumors compared with NOD-*scid* mice. Ten unique primary human colon tumor specimens (7 male and 3 female patients aged 56–73 years) were collected. Tumors were resected from both the right and left side. Rectal cancer specimens were excluded. Distant metastases were absent. Lymph node status and local invasion were not known. Tumor fragments 1 mm × 1 mm in size from seven distinct tumors were implanted SC or under the renal capsule of NOD-*scid* or NSG mice in order to assess the take rate and the fidelity of tumor growth among tumors expanded at two different sites. An additional three distinct tumors were grown in the SC location in NOD-*scid*, NSG and NRG mice in order to assess tumor take rate, tumor size and architectural properties (Fig. 1a, b). Tumor take rate in NOD-*scid* mice was erratic (Fig. 1a), and the sizes of the few observed tumors were widely variable (Fig. 1b). Larger tumor volumes and higher tumor weights were seen in tumors with central necrosis and abscess formation, thus true weight of the tumor parenchyma could not be accurately assessed. In contrast, all tumors grew in NSG and NRG mice, and the percentages of mice that engrafted with each tumor were higher in the NSG and NRG (90 and 91 %) compared to the NOD-scid model (46 %). There was minimal variability in tumor sizes following SC engraftment in NSG and NRG mice.

Figure 1a, b. The average time for tumor growth to a palpable size (0.5–0.75 cm^3) was ~4 weeks in both NSG and NRG mice, and ~8 weeks in NOD-*scid* mice (though not all tumors grew in the NOD-*scid* even when observed to 12 weeks).

Human Colon Tumor Architecture Is Preserved in the NSG and NRG Mice

In order to serve as a valid model of human tumor growth, the architecture of the original tumor (Fig. 2a) must be maintained within recipient mice with regard to retention of gland structure, location and distribution of fibroblasts

A Tumor growth in NOD *scid*, NSG and NRG mice by location

		Subcutaneous			Subrenal capsule		
		NOD *scid*	NSG	NRG	NOD *scid*	NSG	NRG
○	1	0/10	10/10	ND	5/10	10/10	ND
	2	ND	3/4	ND	4/5	5/5	ND
●	3	6/10	10/10	ND	6/10	6/6	ND
●	4	0/10	10/10	ND	0/10	10/10	ND
	5	2/2	5/7	ND	1/5	5/5	ND
	6	ND	5/5	ND	6/10	10/10	ND
	7	ND	7/12	9/12	5/8	8/8	ND
▲	8	10/10	10/10	10/10	9/10	10/10	10/10
△	9	8/10	7/7	7/7	7/10	5/5	5/5
▲	10	3/10	6/6	6/6	1/10	4/4	4/4

B Subcutaneous tumor weight

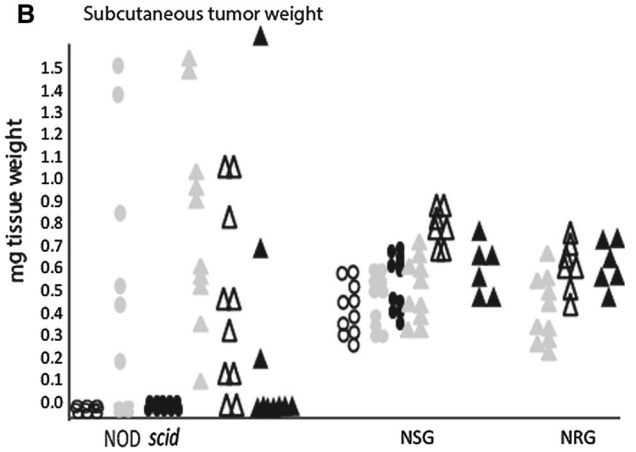

Fig. 1 Growth characteristics of human colon cancer in NOD-*scid*, NSG and NRG mice. **a** Human colon cancer placed SC or in the subrenal capsule space in the strain of mouse indicated. Number of mice per group as listed. The tumor "take rate" was defined as the number of mice with palpable tumors at 4–12 weeks. **b** Tumor weight at 4 weeks in six representative cohorts as marked in **a**. *Note* tumors in NOD-*scid* mice were associated with marked necrosis and abscess formation accounting for the higher tumor weight. Symbols in **a** identify the tumor which is graphed in **b**. *ND* not done

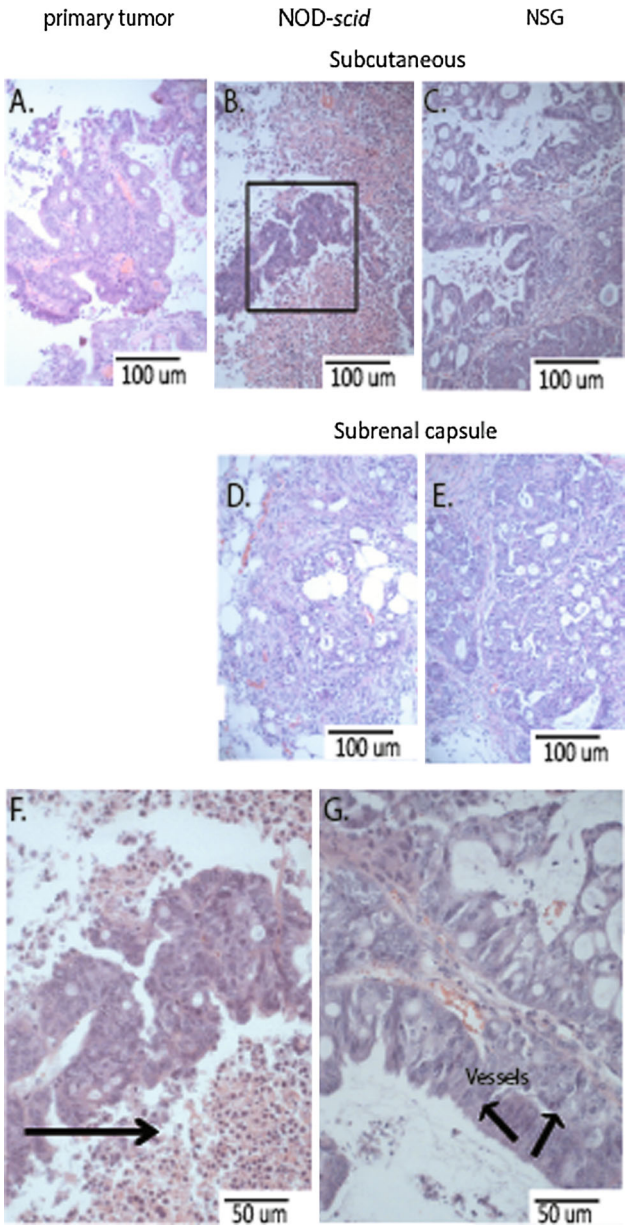

Fig. 2 Histological characteristics of human colon cancer grown in NSG and NRG mice. **a** Primary tumor received from the OR. Primary tumor grown SC in NOD-*scid* (**b**, *boxed area* shown in **f**), or NSG mice (**c**). The same tumor sample was grown in the subrenal capsule of NOD-*scid* (**d**) or NSG (**e**) mice. **f** Enlarged view of **b** to show detail. *Arrow* neutrophilic infiltrate. **g** Enlarged view of **c** to show detail. *Arrows* blood vessels

and blood vessels within the stroma and the relative distribution of tumor-associated immune cells. Tumors implanted SC into NOD-*scid* mice (Fig. 2b, d, f) frequently became necrotic. Few tumors were grossly intact with architectural distortion observed in stained sections, while the majority of tumors were grossly distorted with a thin rim of tumor surrounding a central core of inflammatory cells and debris. Varying levels of host-versus-graft reaction were present in all samples with inflammatory infiltrates surrounding tumors, as well as infiltrating and destroying gland structure and tumor architecture. Gross observation revealed that gland structure was lost and blood vessels were not identified within the tumor. In contrast, colon tumors implanted in NSG and NRG mice maintained uniform architecture and gland structure. Gland structure, nuclear orientation, goblet cells and distribution of stroma were indistinguishable between tumors implanted in NSG and NRG mice (not shown) and the patient tumor (Fig. 2c). The few infiltrating cells that were

observed were in a similar pattern and distribution when compared to the parent tumor.

Colon tumors implanted under the renal capsule of NSG and NRG mice had a similar growth rate as the SC tumors, and similar architectural characteristics. In contrast, tumors implanted under the renal capsule of NOD-*scid* mice grew poorly and were necrotic with host cell infiltrate, loss of stroma and architectural distortion. Tumors grown in NSG and NRG mice grew uniformly, had no identifiable host cell infiltrate, and had abundant stroma. Although gland structure was observed in tumors grown in NOD-*scid* mice, it did not closely resemble the patient tumor. Because of this and because the SC tumor induces less host stress to implant compared to invasive surgery required for engraftment under the renal capsule, permits visual and tactile monitoring of tumor growth rate, and can easily be harvested, we chose to pursue the SC site of tumor growth in our subsequent studies.

Within Colon Cancer Tumors, Tumor Cells Actively Proliferate and the Stroma Is Mitotically Inactive

Colon cancer epithelial cells were uniformly highly proliferative as determined by staining for PCNA, while stromal fibroblasts, leukocytes and endothelial cells were mitotically inactive and did not stain for PCNA (Fig. 3a, b). SC-implanted tumors in NSG or NRG mice had a similar pattern of PCNA staining, with abundant activity in tumor cells, and little to no staining in the stromal compartment. These results implied that the stroma within the human tumor was not proliferating and as tumors grew, the stroma would be populated by mechanisms other than proliferation of existing cells. Tumors expanded in the mouse maintained similar composition and quantity of stroma relative to tumor cells as seen in the primary tumors and offered us the opportunity to determine whether there was an influx of murine host stromal cells into the human tumor xenografts. Antibodies specific for human vimentin readily recognized the fibroblast pool within the human primary tumor and identified cells intercalating between glands and as larger collections within the tumor stroma (Fig. 4a). At 2 weeks after expansion of the tumors in NSG and NRG mice, the human-derived fibroblast pool declined to ~50 % of stromal fibroblasts (Fig. 4a, c) and declined further to ~25 % by 4 weeks (Fig. 4a, c) when the tumors had reached 0.5–0.75 cm in size in the largest dimension. Tumors expanded in secondary and tertiary hosts did not contain any identifiable human fibroblasts (Fig. 4c), though the size and composition of the tumor stroma remained indistinguishable from the primary tumor removed from the patient with the human fibroblasts having been replaced by mouse fibroblasts (Fig. 4). We confirmed the mouse stromal cells were fibroblasts by a combination of human/mouse and human-specific α-SMA immunostaining. First-generation human colon tumors expanded in the NSG mouse stained with antibody directed against human α-SMA (data not shown) and human/mouse α-SMA (Fig. 4d). Human colon tumors passaged through the NSG mouse for 11 generations stained with antibody, which recognized both human/mouse α-SMA (Fig. 4e) but not with antibody directed specifically against human α-SMA (Fig. 4f), demonstrating that the mouse stromal cells were fibroblasts. Next, we examined human CD45+ leukocytes within tumors. The primary tumors we collected had minimal leukocyte infiltration, and numbers of human leukocytes declined over time, completely disappearing by the second passage in the mouse (Fig. 4b, c) and later passaged tumors did not stain for human leukocytes (Fig. 4b, c).

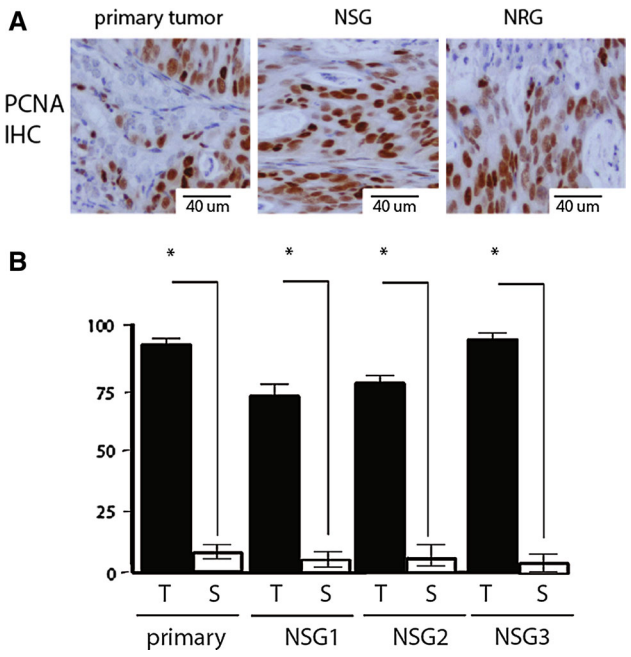

Fig. 3 Tumor epithelial cells are highly proliferative, while stromal cells are relatively quiescent. PCNA staining of **a** primary colon tumor samples and colon tumor expanded in the NSG and NRG models (as labeled). **b** Percent PCNA-positive nuclei in the tumor epithelial cells (*T*) and the stromal cells (*S*) in the primary tumor (*primary*) or from three separate tumors harvested from individual NSG and NRG mice (SC location). Four high-power fields per tumor evaluated, with a minimum of 100 cells per cell type. Four distinct tumors evaluated. Mean ± 1 SD. $*P < 0.02$

Stroma Within Implanted Tumors Undergoes Continuous Turnover

We next addressed if the human stroma was a static component of the tumor, or if mouse cells were recruited as the tumor expands. We first implanted and expanded human colon cancer fragments in NSG mice and then

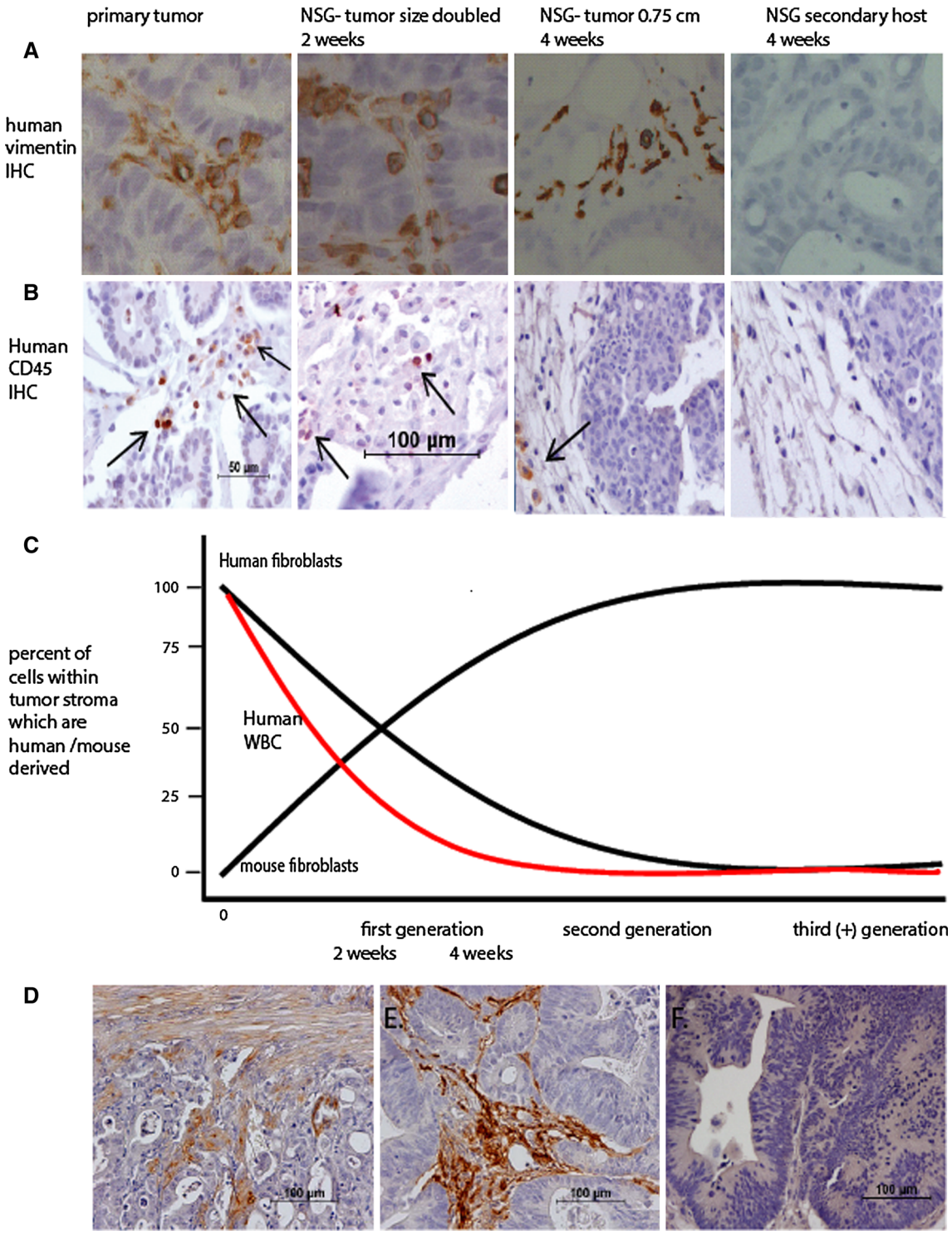

transplanted the tumors into secondary NSG–GFP hosts in order to track the influx of GFP-positive stromal cells. IHC directed against GFP was used to localize GFP-positive cells within tumors. Tumors implanted into non-GFP expressing NSG mice, as expected, failed to stain with anti-GFP antibody. Tumors implanted into GFP expressing NSG mice were repopulated with GFP expressing stroma. As early as 2 weeks after tumor transfer, the stroma within the tumor was of the new host (GFP-positive) origin (Fig. 5c, d). Subsequent transfer of the tumor into a non-GFP expressing host resulted in the GFP expressing stroma rapidly being replaced with non-GFP stroma such that by 2

◀**Fig. 4** Human fibroblasts in colon tumor stroma are replaced by mouse-derived fibroblasts. **a** Antibody directed against human vimentin uniformly stains stroma in primary human colon cancer specimen. Primary tumor implanted into NSG mice and grown for 2 weeks has human stroma mixed with mouse stroma (histologically defined fibroblast cells that failed to stain with antihuman vimentin Ab). At 4 weeks, approximately 25 % of the stroma is human derived, and after passage through a second host no human fibroblasts are recovered (*panels* as labeled). **b** Staining for human CD45 in primary tumor, tumor grown for 2 weeks in the NSG mouse, tumor grown for 4 weeks in the NSG mouse or passaged into a second NSG host (*panels* as labeled) demonstrate a similar decline in human WBC. **c** Schematic representation of stromal cell turn over in human colon cancer expanded in the NSG mouse model; fibroblasts (*black line*) and leukocytes (*red line*) from human and mouse as labeled. Three tumors at each time point were evaluated; five sections per tumor; four high-power fields (×60) per section. A minimum of 100 cells were counted per tumor, and scores were averaged to generate a single number per time point and a graph generated to incorporate the "best fit" curve. **d** First-generation human colon tumor expanded in the NSG mouse, stained with antibody against human alpha SMA. Human colon tumor expanded through 11 generations of NSG mice, stained with antibody which recognizes **e** both human and mouse alpha SMA or **f** only human alpha SMA. Positive cells stain *brown*

weeks, only rare GFP expressing cells were observed (data not shown).

Human Colon Tumors Expanded in NSG and NRG Mice Respond to Standard 5-FU Chemotherapy

There was a significant decrease in the total WBC count after 7 (data not shown) and 14 days of 5-FU treatment, while the hematocrit and hemoglobin levels remained stable (Fig. 6). There was no gross evidence of active infection during this time in any of the mice. Histological appearance of the small intestine, colon and liver of the NSG and NRG mice receiving 5-FU was indistinguishable from that of NOD-*scid* receiving the same dose (data not shown). Once SC-implanted human colon cancer fragments had reached a palpable size in NSG and NRG mice, the mice were weighed and tumor volumes were measured. 5-FU at a dose of 5 mg/kg or vehicle alone (control mice) was injected ip daily for 14 consecutive days. As expected, WBC levels declined in 5-FU-treated mice but not in control mice receiving vehicle alone. Animal weights and tumor sizes did not differ between treated and untreated groups (data not shown). However, histological evaluation of the tumors showed a dramatic effect of 5-FU on tumor architecture and cell viability. After 2 weeks of 5-FU treatment, gland structure was lost and the original organized glands were replaced with necrotic cells, leukocyte infiltrate and cellular debris (Fig. 7a–c). PCNA staining of tumor sections demonstrates that most of the proliferating cells were eliminated by chemotherapy, and VEGF staining shows near complete loss of blood vessels within tumors (Fig. 7a–c).

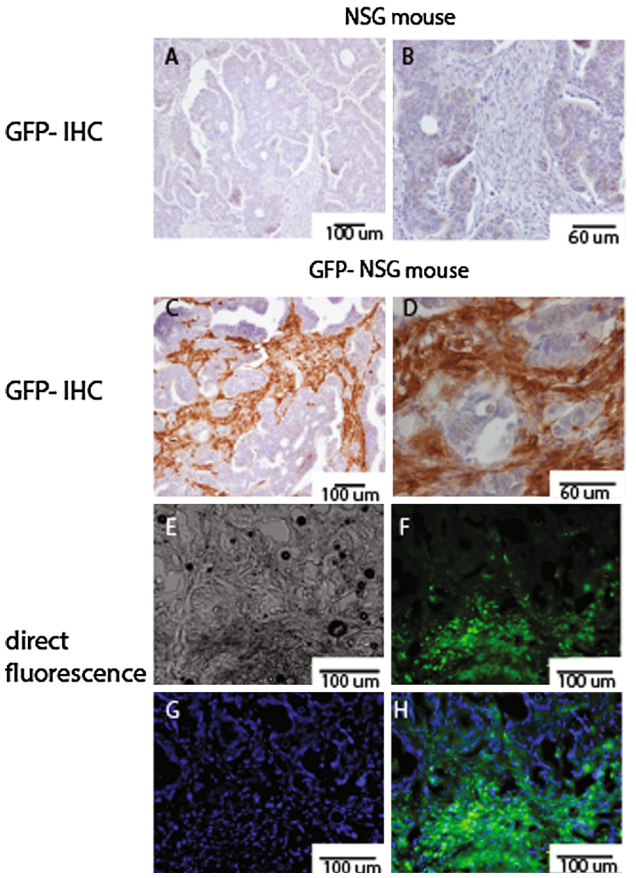

Fig. 5 Stromal repopulation of tumors is a dynamic process. Colon tumors grown in an NSG (non-GFP) mouse were harvested and placed into second NSG recipient mice; **a** low-power, **b** high-power views of IHC directed against GFP in a NSG (non-GFP) mouse, or **c** low-power, **d** high-power view of IHC directed against GFP after transfer of the tumor from NSG mice into a secondary NSG-GFP transgenic host; **e** light microscopy **f** GFP, **g** DAPI **h** merged: tumor in the NSG-GFP host was evaluated for GFP expression by direct fluorescence microscopy on frozen sections of tissue

Discussion

NSG and NRG mice are powerful tools for studying human tissue in a clinically relevant in vivo system. Here, we show that primary human colon cancer tissue can be propagated effectively and rapidly, providing a study platform for investigating tumor–stroma interactions and assessing treatment interventions. Both NSG and NRG mice support uniform rapid growth of human colon tumors, which maintain high histologic fidelity.

Fibroblasts play a pivotal role in tumor biology at all stages of disease and are crucial to any model system which interrogates the tumor stromal interaction [28–31]. Earlier mouse models that support propagation of human tumor explants from surgically resected specimens rely on the NOD-*scid*, C.B–17-*scid* or the nude mouse. These models have a reported primary tumor take rate of

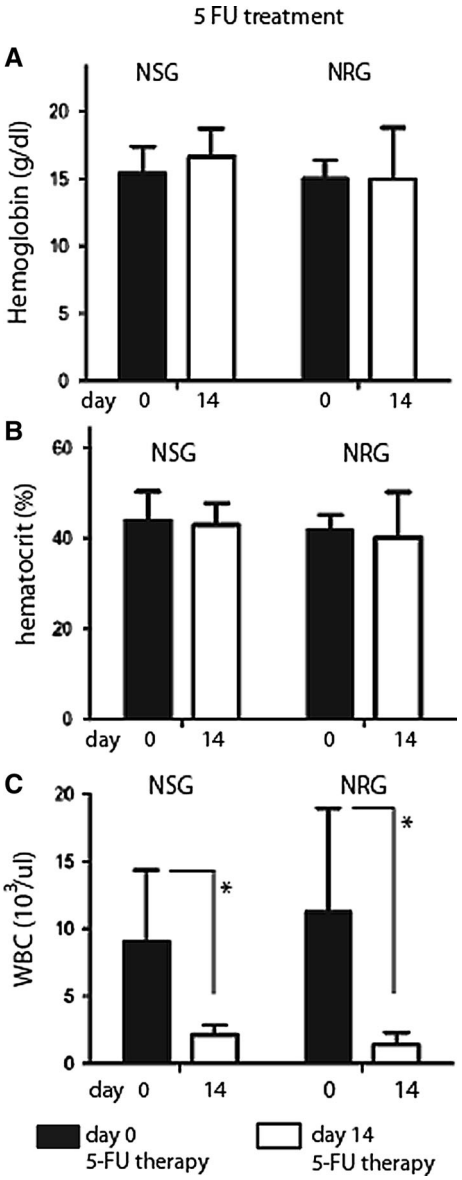

Fig. 6 NSG and NRG mice tolerate 5-FU therapy. NSG and NRG without tumors were given 5 mg/kg 5-FU daily via intraperitoneal injection and peripheral blood assessed at day 0 (prior to therapy) and day 14 **a** hemoglobin, **b** hematocrit and **c** WBC counts were assessed from peripheral blood of NSG and NRG mice as indicated ($N = 6$ per group). Results reported as the mean ± 1 SD. *$P < 0.02$

40–60 % under ideal conditions, and success depends upon the primary tumor type [13, 14], size of the tissue fragment and the location of the implant. For colon cancer propagation, the NOD-*scid* model is superior to the nude mouse model [12]. However, a substantial drawback to the NOD-*scid* mouse is a relatively intact innate immune system, including functional NK cells, which mount a significant host-versus-graft response resulting in architectural destruction, tumor cell necrosis, loss of stroma and often complete rejection of the tumor xenograft. In addition to the NOD-*scid* and nude mouse models, NOD-*Rag1*^{null} mice have been used as models of colon cancer [32]. NOD-*scid* and NOD-*Rag1*^{null} mice are similar with an important caveat. The *scid*, *Rag1*^{null} *and Rag2*^{null} mutations prevent the genetic recombination required for functional B- and T-cell receptors, resulting in similar immune defects. However, the *scid* mutation is broadly expressed and significantly impacts DNA repair in all tissue, while *Rag1*^{null} *and Rag2*^{null} mice exhibit defects restricted to recombination within T- and B-cell receptors. Because of these differences, NSG mice are sensitive to radiation and potentially drug-induced DNA damage, while NRG mice are relatively radio resistant. Though not affecting tumor take rates or growth kinetics, these differences could greatly impact the effects of chemotherapy with radiomimetic drugs and radiation treatment, thus requiring careful consideration of the models chosen for a given therapeutic question.

Consistent with what has been shown for other tumor types [19, 20] and [31], we show here that human colon cancer fragments engraft in the NSG and NRG mice offer the unique feature of stromal replacement with mouse-derived cells over time and tumor passage. Stroma–tumor interaction is recognized as integral for tumor growth [33] and is a unique target for cancer therapy. NSG and the NRG mice provide models where one can manipulate the stroma–tumor cell interaction, thus directly testing the impact of select signaling pathways on tumor growth and invasion. We show that once transplanted into NSG and NRG mice, the human colon cancer epithelial cells remain proliferative while the human stromal cells remain quiescent. As the tumor expands in size, the human fibroblast population is replaced by mouse-derived fibroblasts until the entire stroma is mouse derived. Further, this stromal cell population is not static, but rather is in flux, and is consistently turned over by the recruitment and incorporation of new mouse cells. The source of the stromal cells in human tumors, and subsequently in the tumors expanded in the mouse, is not known [34–38].

The NRG and NSG mouse models offer a powerful system in which to address the enigma of stromal cell origin and the dependence of the tumor on its stroma. Additionally, the efficacy of therapies can be assessed in a clinically relevant and easily manipulated model.

We speculate the NSG and NRG models will greatly enhance the ability to test new agents, design additional therapeutic approaches and tailor therapy to individual tumor types [39–41]. These models will allow testing of multiple compounds simultaneously in a single-tumor sample, thus allowing head to head comparison of agents. They will also allow the identification of subsets of tumors that may selectively respond to an agent based on histology, gene structure or gene expression, thus allowing

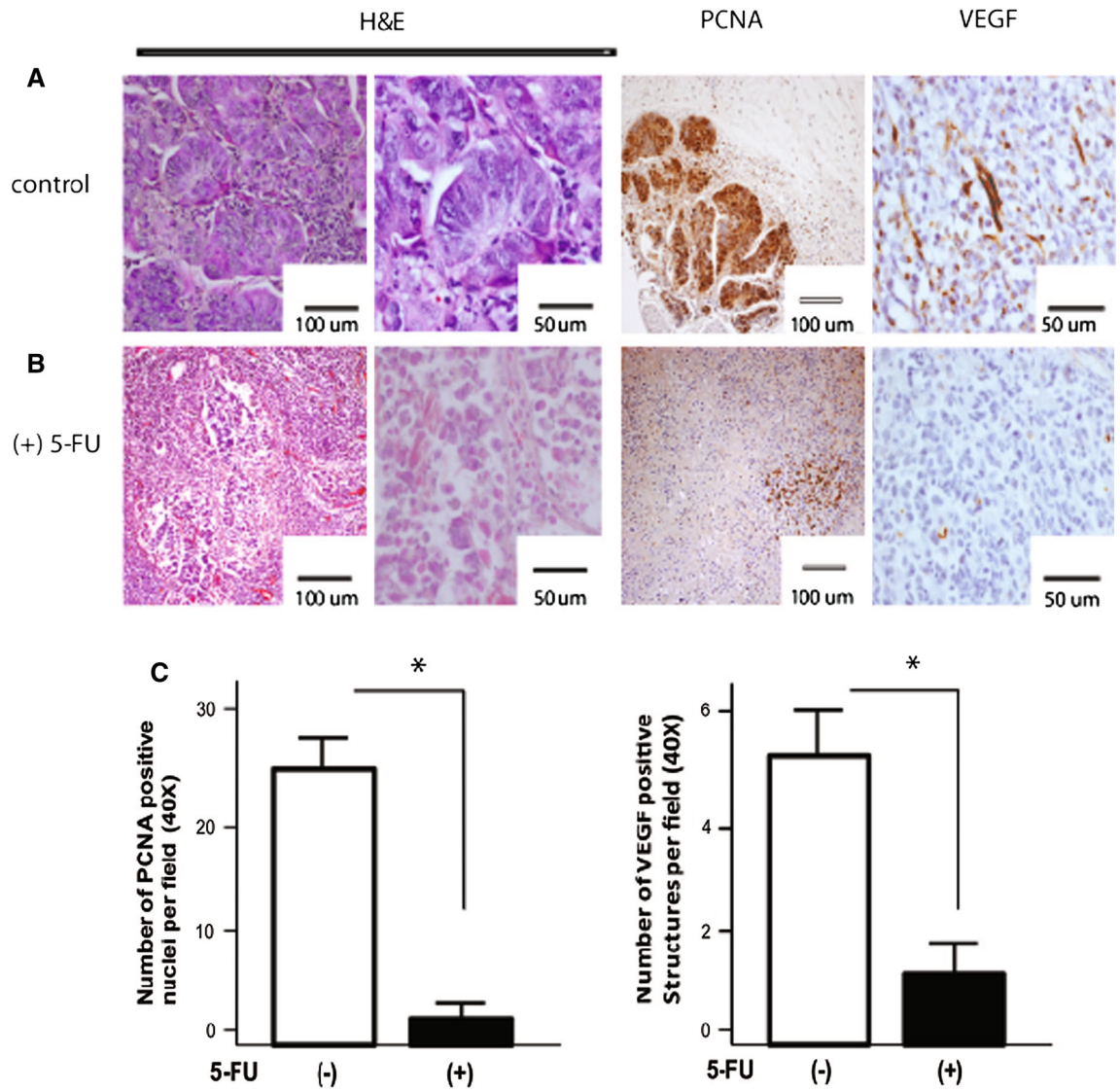

Fig. 7 5-FU therapy effectively kills human colon cancer cells in NRG mice. NRG mice bearing human colon cancer xenografts were treated with **a** vehicle (control) or **b** 5-FU; 5 mg/kg daily for 2 weeks. H&E staining, anti-PCNA (stains both human and mouse) and anti-VEGF (stains both human and mouse) IHC are shown as labeled. **c** Numbers of PCNA- and VEGF-positive cells per ×40 field in treated and untreated samples as labeled

focused patient selection during design of subsequent clinical trials. Tumor characteristics between mice implanted at the same time are relatively uniform and allow significant results from a small number of animals. These models offer the ability to simultaneously test multiple intervention strategies in an in vivo system that closely approximates the human tumor environment.

In addition to promising use in drug discovery and preclinical evaluation, we suggest that the NSG and NRG models have substantial promise for personalized approaches to chemotherapy. In these mice, the interval between colon tumor implantation and palpable growth is relatively short, with palpable tumor size reached in approximately 4 weeks, allowing intervention studies to be performed in the time frame that a patient would be recovering from surgery. Additionally, multiple and combination agents can be tested and treatments tailored to a patient's specific tumor genotype and/or phenotype can be pursued, allowing personalized medicine in a time frame that has clinical relevance. The ability to passage a patient's tumor to successive generations of mice without loss of architecture or growth properties raises the unique possibility of testing second- or third-line intervention if initial therapy fails, or if tumor recurrence is encountered. Indeed, personalized cancer therapy, in which treatment is specific for an individual patient's tumor, will theoretically be more effective and provide better outcome [42–47]. The NSG and NRG mouse model allows rigorous and robust testing of multiple

agents in a patient-specific fashion, making the notion of personalized therapy a reality.

Thus, the NSG and NRG mouse models offer three distinct advantages over present models of colon cancer. First, within the NSG and NRG mouse models, the dynamics of stromal replacement permits analyses of tumor cell–stromal cell cross-talk that can be precisely interrogated and manipulated. Second, therapeutics can be tested potentially shortening the time from bench discovery to bedside intervention. Third, patient-specific tumor response to therapeutics can guide personalized medicine approaches for individual patient care.

Acknowledgments Grant support: NIH CA119061 (JH), CA034 196 (LDS) and CA034196, AI46629, and the Helmsley Charitable Trust (DLG).

Conflict of interest None.

References

1. Casazza A, Di Conza G, Wenes M, et al. Tumor stroma: a complexity dictated by the hypoxic tumor microenvironment. *Oncogene*. 2013;33:1743–1754.
2. Hemmings C. Is carcinoma a mesenchymal disease? The role of the stromal microenvironment in carcinogenesis. *Pathology*. 2013;45:371–381.
3. Noble P, Vyas M, Al-Attar A, et al. High levels of cleaved caspase-3 in colorectal tumour stroma predict good survival. *Br J Cancer*. 2013;108:2097–2105.
4. Palumbo A Jr, Ferreira LB, Reis de Souza PA, et al. Extracellular matrix secreted by reactive stroma is a main inducer of pro-tumorigenic features on LNCaP prostate cancer cells. *Cancer Lett*. 2012;321:55–64.
5. Bhowmick NA, Moses HL. Tumor-stroma interactions. *Curr Opin Genet Dev*. 2005;15:97–101.
6. Kaplan RN, Riba RD, Zacharoulis S, et al. VEGFR1-positive haematopoietic bone marrow progenitors initiate the pre-metastatic niche. *Nature*. 2005;438:820–827.
7. Robert J. Biology of cancer metastasis. *Bull Cancer*. 2013;100: 333–342.
8. Yu B, Chen X, Li J, et al. Stromal fibroblasts in the microenvironment of gastric carcinomas promote tumor metastasis via upregulating TAGLN expression. *BMC Cell Biol*. 2013;14:17.
9. O'Brien CA, Pollett A, Gallinger S, et al. A human colon cancer cell capable of initiating tumour growth in immunodeficient mice. *Nature*. 2007;445:106–110.
10. Ricci-Vitiani L, Lombardi DG, Pilozzi E, et al. Identification and expansion of human colon-cancer-initiating cells. *Nature*. 2007;445: 111–115.
11. Shmelkov SV, Butler JM, Hooper AT, et al. CD133 expression is not restricted to stem cells, and both CD133+ and CD133− metastatic colon cancer cells initiate tumors. *J Clin Invest*. 2008;118:2111–2120.
12. Morikawa K, Walker SM, Nakajima M, et al. Influence of organ environment on the growth, selection, and metastasis of human colon carcinoma cells in nude mice. *Cancer Res*. 1988;48:6863–6871.
13. Kubota T, Yamaguchi H, Watanabe M, et al. Growth of human tumor xenografts in nude mice and mice with severe combined immunodeficiency (SCID). *Surg Today*. 1993;23:375–377.
14. Priolo C, Agostini M, Vena N, et al. Establishment and genomic characterization of mouse xenografts of human primary prostate tumors. *Am J Pathol*. 2010;176:1901–1913.
15. Tanaka Y, Wu AY, Ikekawa N, et al. Inhibition of HT-29 human colon cancer growth under the renal capsule of severe combined immunodeficient mice by an analogue of 1,25-dihydroxyvitamin D3, DD-003. *Cancer Res*. 1994;54:5148–5153.
16. Shultz LD, Pearson T, King M, et al. Humanized NOD/LtSz-scid IL2 receptor common gamma chain knockout mice in diabetes research. *Ann N Y Acad Sci*. 2007;1103:77–89.
17. Shultz LD, Brehm MA, Garcia-Martinez JV, et al. Humanized mice for immune system investigation: progress, promise and challenges. *Nat Rev Immunol*. 2012;12:786–798.
18. Li M, Zhou M, Gong M, et al. A novel animal model for bone metastasis in human lung cancer. *Oncol Lett*. 2012;3:802–806.
19. Simpson-Abelson MR, Sonnenberg GF, Takita H, et al. Long-term engraftment and expansion of tumor-derived memory T cells following the implantation of non-disrupted pieces of human lung tumor into NOD-scid IL2Rgamma(null) mice. *J Immunol*. 2008;180:7009–7018.
20. Quintana E, Shackleton M, Sabel MS, et al. Efficient tumour formation by single human melanoma cells. *Nature*. 2008;456: 593–598.
21. Bankert RB, Balu-Iyer SV, Odunsi K, et al. Humanized mouse model of ovarian cancer recapitulates patient solid tumor progression, ascites formation, and metastasis. *PLoS ONE*. 2011;6: e24420.
22. Saito Y, Yuki H, Kuratani M, et al. A pyrrolo-pyrimidine derivative targets human primary AML stem cells in vivo. *Sci Transl Med*. 2013;5:181ra52.
23. Agliano A, Martin-Padura I, Mancuso P, et al. Human acute leukemia cells injected in NOD/LtSz-scid/IL-2Rgamma null mice generate a faster and more efficient disease compared to other NOD/scid-related strains. *Int J Cancer*. 2008;123:2222–2227.
24. Cao Z, Liao L, Chen X, et al. Enhancement of antitumor activity of low-dose 5-fluorouracil by combination with Fuzheng-Yiliu granules in hepatoma 22 tumor-bearing mice. *Integr Cancer Ther*. 2013;12:174–181.
25. Cheng CY, Lin YH, Su CC. Anti-tumor activity of Sann–Joong–Kuey–Jian–Tang alone and in combination with 5-fluorouracil in a human colon cancer colo 205 cell xenograft model. *Mol Med Rep*. 2010;3:227–231.
26. Yoshioka T, Wada T, Uchida N, et al. Anticancer efficacy in vivo and in vitro, synergy with 5-fluorouracil, and safety of recombinant methioninase. *Cancer Res*. 1998;58:2583–2587.
27. Lee M, Pierce A, Mahaffey W, et al. Interleukin-2 in neoadjuvant therapy potentiates inhibitory activity of 5-fluorouracil and interferon in experimental liver metastases. *Anticancer Drugs*. 1994;5:239–243.
28. Ernst M, Ramsay RG. Colorectal cancer mouse models: integrating inflammation and the stroma. *J Gastroenterol Hepatol*. 2012;27:39–50.
29. Bhowmick NA, Neilson EG, Moses HL. Stromal fibroblasts in cancer initiation and progression. *Nature*. 2004;432:332–337.
30. Houghton J, Li H, Fan X, et al. Mutations in bone marrow-derived stromal stem cells unmask latent malignancy. *Stem Cells Dev*. 2010;19:1153–1166.
31. Shultz L, Goodwin N, Ishikawa F, et al. Human cancer growth and therapy in immunodeficient mouse models. In: Abate-Shen

C, Politi K, Chodosh L, Olive KP, editors. *Mouse models of cancer: a laboraory manual*. Cold Spring Harbor, NY: Cold Spring Harbor Laboratory Press; 2013.
32. Fox JG, Ge Z, Whary MT, et al. Helicobacter hepaticus infection in mice: models for understanding lower bowel inflammation and cancer. *Mucosal Immunol*. 2011;4:22–30.
33. Li H, Fan X, Houghton J. Tumor microenvironment: the role of the tumor stroma in cancer. *J Cell Biochem*. 2007;101:805–815.
34. Iwano M, Plieth D, Danoff TM, et al. Evidence that fibroblasts derive from epithelium during tissue fibrosis. *J Clin Invest*. 2002;110:341–350.
35. Direkze NC, Hodivala-Dilke K, Jeffery R, et al. Bone marrow contribution to tumor-associated myofibroblasts and fibroblasts. *Cancer Res*. 2004;64:8492–8495.
36. Kuperwasser C, Chavarria T, Wu M, et al. Reconstruction of functionally normal and malignant human breast tissues in mice. *Proc Natl Acad Sci USA*. 2004;101:4966–4971.
37. Worthley DL, Si Y, Quante M, et al. Bone marrow cells as precursors of the tumor stroma. *Exp Cell Res*. 2013;319:1650–1656.
38. Sartore-Bianchi A, Ricotta R, Cerea G, et al. Rationale and clinical results of multi-target treatments in oncology. *Int J Biol Markers*. 2007;22:S77–S87.
39. Demichele A, Berry DA, Zujewski J, et al. Developing safety criteria for introducing new agents into neoadjuvant trials. *Clin Cancer Res*. 2013;19:2817–2823.
40. Martell RE, Sermer D, Getz K, et al. Oncology drug development and approval of systemic anticancer therapy by the U.S. Food and Drug Administration. *Oncologist*. 2013;18:104–111.
41. Cho SH, Jeon J, Kim SI. Personalized medicine in breast cancer: a systematic review. *J Breast Cancer*. 2012;15:265–272.
42. Dammann M, Weber F. Personalized medicine: caught between hope, hype and the real world. *Clinics (Sao Paulo)*. 2012;67:91–97.
43. Fenstermacher DA, Wenham RM, Rollison DE, et al. Implementing personalized medicine in a cancer center. *Cancer J*. 2011;17:528–536.
44. Gonzalez de Castro D, Clarke PA, Al-Lazikani B, et al. Personalized cancer medicine: molecular diagnostics, predictive biomarkers, and drug resistance. *Clin Pharmacol Ther*. 2013;93:252–259.
45. Lisanti MP, Martinez-Outschoorn UE, Pavlides S, et al. Accelerated aging in the tumor microenvironment: connecting aging, inflammation and cancer metabolism with personalized medicine. *Cell Cycle*. 2011;10:2059–2063.
46. Maitland ML, Schilsky RL. Clinical trials in the era of personalized oncology. *CA Cancer J Clin*. 2011;61:365–381.
47. Mi Q, Li NY, Ziraldo C, et al. Translational systems biology of inflammation: potential applications to personalized medicine. *Pers Med*. 2010;7:549–559.